

Lyman- α power spectrum as a probe of modified gravity

Philippe Brax,^a Patrick Valageas^a

^aInstitut de Physique Théorique, Université Paris-Saclay, CEA, CNRS,
F-91191 Gif sur Yvette, France

E-mail: philippe.brax@ipht.fr, patrick.valageas@ipht.fr

Abstract. We investigate the impact of modified-gravity models on the Lyman- α power spectrum. Building a simple analytical modeling, based on a truncated Zeldovich approximation, we estimate the intergalactic medium power spectrum and the Lyman- α flux decrement power spectrum along the line of sight. We recover the results of numerical simulations for $f(R)$ -gravity models and present new results for K-mouflage scenarios. We find that the shape of the distortion due to the modified gravity depends on the model, through the scale-dependence or not of their growth rate. This is more clearly seen in the three-dimensional power spectrum than in the one-dimensional power spectrum, where the line-of-sight integration smoothes the deviation. Whilst the Lyman- α power spectrum does not provide competitive bounds for $f(R)$ theories, it could provide useful constraints for the K-mouflage models. Thus, the efficiency of the Lyman- α power spectrum as a probe of modified-gravity scenarios depends on the type of screening mechanism and the related scale dependence it induces. The prospect of a full recovery of the three-dimensional Lyman- α power spectrum from data would also lead to stronger constraints and a better understanding of screening mechanisms.

Contents

1	Introduction	1
2	Cosmological scenarios	2
2.1	f(R) theories	3
2.2	K-mouflage models	4
3	Flux probability distribution function	5
3.1	Modeling $\mathcal{P}(F)$	5
3.2	$\mathcal{P}(\delta_s)$ for modified-gravity theories	6
3.3	$\mathcal{P}(F)$ for modified-gravity theories	8
4	Lyman-α flux decrement power spectrum	10
4.1	IGM power spectrum $P_{\text{IGM}}(k)$	10
4.2	Matter power spectrum for modified-gravity theories	12
4.3	Lyman- α power spectrum $P_{\delta_F}(k)$	13
4.4	Lyman- α power spectrum for modified-gravity theories	16
4.5	Degeneracies with physical parameters	18
5	Conclusion	19
A	Cumulant generating function	20
B	Second-order perturbation theory	20
C	The Zeldovich approximation	21

1 Introduction

Soon after the discovery of the acceleration of the expansion of the Universe, the possibility that modified gravity on cosmological scales could be at the origin of this late time acceleration was raised [1]. This led to a renewed interest in massive gravity [2, 3], which gives a tantalising link between the amount of dark energy necessary to generate the acceleration of the Universe and the graviton mass. Another class of models involving a new scalar field, akin to the scalar polarisation of massive gravity, could also lead to self-tuned [4] acceleration using the Horndeski [5, 6] (and beyond) [7] classification of trouble-free scalar theories in four dimensions. In both cases, the number of theories passing the stringent constraint on the speed of gravitational waves is extremely limited [8–10]. In this paper, we shall focus on models which do not tackle the acceleration issue per se. They all contain a vacuum energy which is partially responsible for the late-time acceleration. On the other hand, gravity is still modified and constrained on large cosmological scales. We concentrate on models of the $f(R)$ type for which the astrophysical constraints imply that deviations from the Λ -CDM template are limited [11]. Nevertheless, for models of the K-mouflage type [12], where large clusters are not screened [13] and see the effects of the scalar field with no suppression, large-scale observables such as the Lyman- α forest are of relevance.

Such a type of modified gravity has mostly been studied on large linear scales through its impact on the cosmic microwave background (CMB) anisotropies (in particular the integrated Sachs-Wolfe effect), on weak lensing cosmic shear statistics, on the matter power spectrum; and on small nonlinear scales through the matter power spectrum, the abundance of virialized halos and clusters of galaxies. However, very few studies have considered the impact on the Lyman- α forest statistics, see for instance [14] for a work focusing on $f(R)$ -gravity using numerical simulations. In contrast, the Lyman- α power spectrum has become a useful probe of dark matter candidates [15–19], providing constraints on warm dark matter scenarios that suppress the matter power spectrum on small scales because of their non-negligible velocity dispersion. More generally, the Lyman- α power spectrum is a probe of the linear matter power spectrum and of the background cosmology [20–23]. Therefore, it is worth investigating whether the Lyman- α power spectrum could also provide useful constraints on modified gravity. In particular, to pass Solar System tests of gravity, modified-gravity scenarios must include screening mechanisms that ensure convergence to General Relativity in high-density and small-scale environments. Depending on the model, screening may even apply up to galactic or cluster scales. In contrast, Lyman- α forest clouds, which correspond to weakly nonlinear density fluctuations and scales greater than virialized objects, should not be screened. Moreover, being in the weakly nonlinear regime, Lyman- α statistics could be better probes of the linear power spectrum than highly nonlinear scales, which are difficult to predict and involve complex effects, such as baryonic feedback or virialization processes, that can be degenerate with modified-gravity impacts or partly damp the sensitivity to linear modified-gravity effects. In addition, modified-gravity models often induce a new scale dependence for the matter power spectrum, which is typically enhanced as compared with the Λ CDM prediction instead of being suppressed as in warm dark matter scenarios, that could also modify the shape of the Lyman- α power spectrum.

In this paper, we present a first step to estimate the impact of modified-gravity scenarios on the Lyman- α power spectrum. We briefly describe in section 2 the $f(R)$ and K-mouflage theories that we investigate in this paper. Then, we first consider the probability distribution function (PDF) $\mathcal{P}(F)$ of the Lyman- α flux in section 3. We use a standard fluctuating Gunn-Peterson approximation and estimate the impact of modified-gravity theories through their amplification of the growth of matter fluctuations. We find that the effect on the small-scale IGM physics remains modest. Then, we build in section 4 a simple model for the Lyman- α power spectrum. It is based on a truncated Zeldovich approximation, which encodes the dependence on cosmology, and bias parameters that we keep fixed to simplify the analysis. We check that it provides a reasonable match to numerical simulations and observations, in the case of the concordance Λ CDM cosmology. Next, we apply this modeling to the modified-gravity scenarios. We check that we recover the results of numerical simulations [14] for $f(R)$ theories, and we present new results for K-mouflage models. We discuss the impact of these modified-gravity scenarios and we conclude in section 5.

2 Cosmological scenarios

To investigate the possible impact of modified-gravity scenarios on Lyman- α forest statistics, we consider in this paper two well-studied examples, the $f(R)$ theories and the K-mouflage models. We will assume that the variations of the various parameters (such as the IGM temperature) that define the mapping between the matter density field and the Lyman- α statistics can be neglected. Thus, we focus on the deviations that directly arise from the

change of the underlying matter power spectrum and the growth of structures. In a more accurate computation, we can expect the parameters that describe the small-scale hydrodynamics of the Lyman- α forest to show some dependence on the underlying gravitational theory, as they must be related to the formation of large-scale structures. However, in practice some of these parameters are marginalized over as nuisance parameters, or are directly measured from observations, such as the IGM temperature, and can be taken as external fixed inputs. A detailed study of this issue would require dedicated numerical simulations. In this paper, we adopt a simple approach where we assume the main dependence on cosmology to arise from the direct dependence on the large-scale matter distribution and we use the numerical simulations available for the standard LCDM cosmology and the $f(R)$ theories to check that we recover the correct order of magnitude of the various effects we investigate. In this section, we briefly present the two modified-gravity scenarios that we will consider.

2.1 $f(R)$ theories

The $f(R)$ -gravity theories are already very strongly constrained by cosmological and astrophysical data, but they remain interesting as simple examples of modified-gravity effects on the matter distribution. Moreover, they are the only case where numerical simulations of the Lyman- α power spectrum have been performed [14]. This will allow us to check the validity of our analytical modeling. More specifically, we concentrate on a class of $f(R)$ theories of the Hu-Sawicki [24] type, where the action is given by

$$S_{f(R)} = \frac{1}{16\pi\mathcal{G}_N} \int d^4x \sqrt{-g} f(R) \quad (2.1)$$

with

$$f(R) = R - 2\Lambda^2 - f_{R_0} \frac{R_0^2}{R}, \quad (2.2)$$

where $\Lambda^2/8\pi\mathcal{G}_N$ is the vacuum energy responsible for the late time acceleration of the Universe. Here R_0 is the Ricci curvature of the Universe now. We consider the cases of such $f(R)$ theories with $f_{R_0} = -10^{-4}$, -10^{-5} and -10^{-6} . Let us recall that in the linear regime, the growth of density perturbations is enhanced as compared to the LCDM cosmology. This can be described in the evolution equation of the matter density contrast by an effective Newton constant,

$$\mathcal{G}_N \rightarrow \mathcal{G}_N[1 + \epsilon(k, a)], \quad \epsilon(k, a) = \frac{2\beta^2(a)}{1 + m^2(a)a^2/k^2}, \quad (2.3)$$

where the coupling strength β and the mass m of the new degree of freedom are

$$\beta = \frac{1}{\sqrt{6}}, \quad m(a) = \frac{H_0}{c} \sqrt{\frac{\Omega_{m0} + 4\Omega_{\Lambda0}}{2|f_{R_0}|}} \left(\frac{\Omega_{m0}a^{-3} + 4\Omega_{\Lambda0}}{\Omega_{m0} + 4\Omega_{\Lambda0}} \right)^{3/2} \sim 1 \text{ h/Mpc}. \quad (2.4)$$

Thus, on large scales $k \ll am$ we recover General Relativity and the LCDM cosmology, as $\epsilon \simeq 0$, while on small scales $k \gg am$ Newtonian gravity is amplified by a factor 4/3. On smaller nonlinear scales, nonlinear screening effects come into play and ensure a convergence back to General Relativity. Note that the coupling strength β is fixed and of order unity, and we recover the LCDM cosmology at low $|f_{R_0}|$ by pushing the mass $m(a)$ to infinity.

2.2 K-mouflage models

The K-mouflage models are also scalar-tensor theories, but the additional scalar field is massless and has a nonstandard kinetic term. This provides another simple example of modified-gravity scenarios that includes an alternative screening mechanism. The $f(R)$ theories give rise to the chameleon screening mechanism [25, 26], where the additional scalar field obtains a higher mass in high-density environments, which decreases the range of the fifth force and screens compact objects. In contrast, the K-mouflage screening relies on a derivative screening [12, 27, 28], due to the nonlinearity of the kinetic term, so that the fifth force is damped in regions of large field gradients (or large Newtonian force), which gives rise to a K-mouflage radius around compact objects within which one recovers General Relativity. On large linear scales, from the point of view of the matter distribution, the main difference from the $f(R)$ theories is that the scalar field being massless there is no scale dependence for the linear growing mode, as in the standard Λ CDM cosmology, but only a time-dependent amplification.

The K-mouflage theories are characterised by the coupling strength of the scalar field to matter β_K and a Lagrangian kinetic function $K(\chi)$ that is nonlinear. This function must behave like -1 when the kinetic energy of the scalar field is small in the late-time Universe, to play the role of the cosmological constant. Moreover, it must also satisfy the stringent tests of gravity in the Solar System, like the perihelion advance of the moon [29]. In this paper we take

$$K(0) = -1 \quad \text{and} \quad K'(\chi) = 1 + \frac{K_* \chi^2}{\chi^2 + \chi_*^2}, \quad (2.5)$$

where $\chi = -(\partial\phi)^2/2\mathcal{M}^4$, and \mathcal{M}^4 is the dark energy scale. The first derivative $K'(\chi)$ goes from 1 at low χ , as for the standard kinetic term, to the large value K_* at high χ , which gives rise to the screening mechanism that damps the scalar field gradients and the fifth force in high-density environments. We choose to illustrate our results with $\chi_* = 100$ and $K_* = 1000$. We consider the case of a coupling constant $\beta_K = 0.1$ (the $f(R)$ theories correspond to $\beta_f = 1/\sqrt{6}$ as in Eq.(2.4)), to remain consistent with constraints from Big Bang Nucleosynthesis and the Solar System. In practice, $\bar{K}' \simeq 1$ for the background for $z \lesssim 6$, so that the precise form of $K(\chi)$ does not play any role and our results are set by the value of the coupling β_K . Indeed, in this model clusters of galaxies are still in the unscreened linear regime of the scalar field [13] and this is even more so for the Lyman- α forest clouds. Then, in the linear regime the growth of matter density perturbations can again be described by an effective Newton constant as in Eq.(2.3), but it is now scale independent, with

$$\epsilon(a) = \frac{2\beta_K^2}{K'} \simeq 2\beta_K^2 = 0.02 \quad \text{for} \quad \beta_K = 0.1. \quad (2.6)$$

Thus, the amplitude of the deviation from Newtonian gravity is smaller than in $f(R)$ theories, as $\epsilon = 0.02$ instead of the maximum value $1/3$ reached in $f(R)$ theories. However, it holds on a greater range of scales, nearly up to the horizon and down to a smaller screening radius.

In contrast with the $f(R)$ models, we cannot compare our results to numerical simulations, which remain to be developed. However, on linear scales the K-mouflage scenarios mostly differ from the Λ CDM cosmology by a time-dependent effective Newton constant, without introducing new scales. Therefore, at a qualitative level, we can expect their large-scale physics to remain even closer to the Λ CDM cosmology than for the $f(R)$ theories, and our modeling developed in the next sections should fare as well as for the $f(R)$ theories.

3 Flux probability distribution function

3.1 Modeling $\mathcal{P}(F)$

The first statistics we consider in this paper is the probability distribution function $\mathcal{P}(F)$ of the Lyman- α flux F . In the standard fluctuating Gunn-Peterson approximation [20, 30], the Lyman- α optical depth is proportional to the neutral hydrogen density n_{HI} . For a gas in photoionization equilibrium that is mostly ionized, this is proportional to the square of the density multiplied by a temperature-dependent recombination factor, and for temperatures $T \sim 10^4$ K this gives

$$\tau \propto \rho^2 T^{-0.7} \propto (1 + \delta)^\alpha \quad \text{with} \quad \alpha = 2 - 0.7(\gamma - 1), \quad (3.1)$$

where $(\gamma - 1)$ is the exponent of the gas density-temperature relation. This gives for the Lyman- α flux

$$F = e^{-\tau} = e^{-A(1+\delta)^\alpha}. \quad (3.2)$$

The factor A depends on the HI photoionization rate, which is difficult to measure independently. Following standard practice, we set A by requiring that the mean flux $\langle F \rangle$ matches the observational measurements. The exponent γ is typically $\gamma \simeq 1 - 1.6$ and goes to 1.6 at late times in the case of early reionization [31]. Following observations and numerical simulations [32], we take $\gamma = 1.3$ and $T = 2 \times 10^4$ K at $z = 3$, which gives $\alpha = 1.79$. To relate the Lyman- α flux to the matter distribution through Eq.(3.2), we need to specify the smoothing scale x_s of the density contrast. As in [33, 34], we write the comoving smoothing wave number k_s in terms of the Jeans wave number k_J as

$$k_s = 2.2 k_J \quad \text{with} \quad k_J = \frac{a}{c_s} \sqrt{4\pi \mathcal{G}_N \bar{\rho}}, \quad c_s = \sqrt{\frac{5k_B T}{3\mu m_p}}, \quad (3.3)$$

where a is the scale factor, c_s the sound speed, and $\mu \simeq 0.5$ the mean molecular weight. The factor 2.2 accounts for the fact that the Jeans length was smaller at earlier times, which reduces the damping scale at a given redshift [33], and we take $x_s = \pi/k_s$ for the smoothing radius. Then, neglecting the scatter of the density-flux relation (3.2), we write the flux PDF as

$$\mathcal{P}(F) = \mathcal{P}(\delta_s) \left| \frac{d\delta_s}{dF} \right|. \quad (3.4)$$

We define the density probability distribution function $\mathcal{P}(\delta_s)$ through its cumulant generating function $\varphi_s(y)$ (which is also given by its Laplace transform),

$$\mathcal{P}(\delta_s) = \int_{-\infty}^{\infty} \frac{dy}{2\pi i \sigma_s^2} e^{[y\delta_s - \varphi_s(y)]/\sigma_s^2} \quad \text{with} \quad \varphi_s(y) = - \sum_{n=2}^{\infty} \frac{(-y)^2}{n!} \frac{\langle \delta_s^n \rangle_c}{\sigma_s^{2(n-1)}}, \quad (3.5)$$

As described in appendix A, we take for $\varphi_s(y)$ its early-time or low-variance limit, which is determined by the spherical collapse dynamics, see also [35, 36]. Because the Lyman- α forest probes mildly nonlinear perturbations, the generating function $\varphi_s(y)$ may have already somewhat departed from this quasilinear result. However, this should still provide a more accurate shape than the usual lognormal approximation and it allows us to estimate the impact of modified gravity on the shape of the PDF through higher-order cumulants, beyond the density variance.

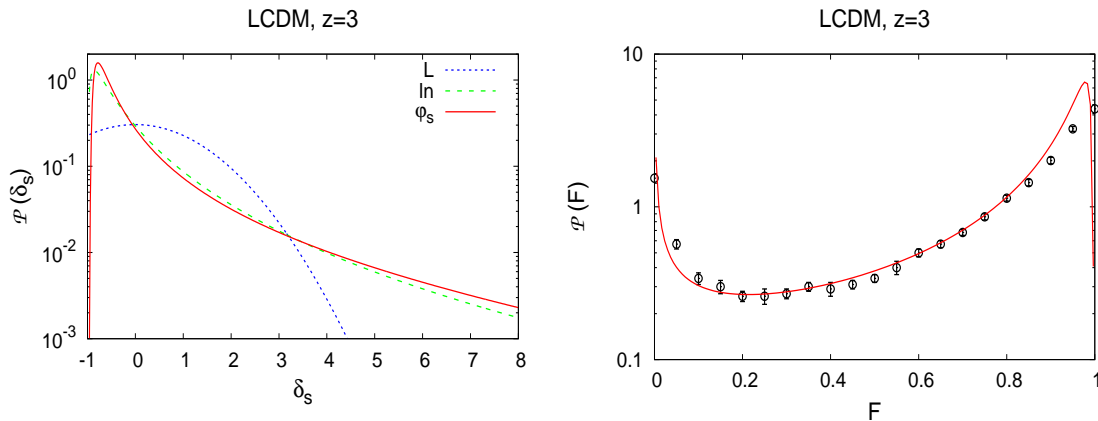


Figure 1. *Left panel:* probability distribution function $\mathcal{P}(\delta_s)$ from Eq.(3.5) (red solid line labeled “ φ_s ”). We also display the Gaussian PDF from linear theory (blue dotted line “L”) and the lognormal approximation (green dashed line “ln”). *Right panel:* Probability distribution function $\mathcal{P}(F)$ from Eq.(3.4). The data points are the observational results of [37].

On the other hand, to be consistent with the approach we use for the Lyman- α power spectrum, we compute the smoothed variance σ_s^2 from the nonlinear truncated Zeldovich power spectrum defined in Eq.(4.2) below. This means that δ_s is the IGM density field associated with the IGM power spectrum (4.1). It differs from the underlying nonlinear matter distribution by the smoothing scale x_s and by the use of the truncated Zeldovich approximation, which provides a reasonable description of the large-scale weakly nonlinear matter distribution while removing the irrelevant contributions from high-density virialized halos that do not contribute to the Lyman- α forest.

We compare in the left panel in Fig. 1 the density PDF (3.5) with the Gaussian PDF from linear theory and the lognormal approximation. We can see that on these mildly nonlinear scales, the density fluctuations of the IGM are modest but the PDF already significantly deviates from the Gaussian, with a peak at a slightly negative density contrast and an extended high-density tail. As is well known, this shape is similar to the usual lognormal approximation.

Next, the mapping (3.2) provides the flux PDF through Eq.(3.4). We can see in the right panel in Fig. 1 that this gives a reasonably good agreement with the observations from [37]. The coefficient A in Eq.(3.2) has been chosen so that the mean flux matches the observed value of [37], $\langle F \rangle = 0.72$, which gives $A \simeq 0.5$.

3.2 $\mathcal{P}(\delta_s)$ for modified-gravity theories

We show in Fig. 2 the relative deviation of the density PDF $\mathcal{P}(\delta_s)$ from the LCDM prediction for the $f(R)$ theories and the K-mouflage model. We consider again the linear Gaussian PDF, the lognormal approximation, and the expression (3.5) that takes into account the nonlinear gravitational dynamics. For the latter, we display the cases when we keep the LCDM function φ_s or use the modified-gravity function $\delta\varphi_s$ (by using the modified-gravity spherical collapse function $\mathcal{F}(\delta_{Lq})$ in Eq.(A.2) in appendix A). The modified-gravity scenarios studied in this paper amplify the growth of density perturbations at low redshifts. This increases the variance σ_s^2 and makes structure formation appear further advanced than in the LCDM cosmology.

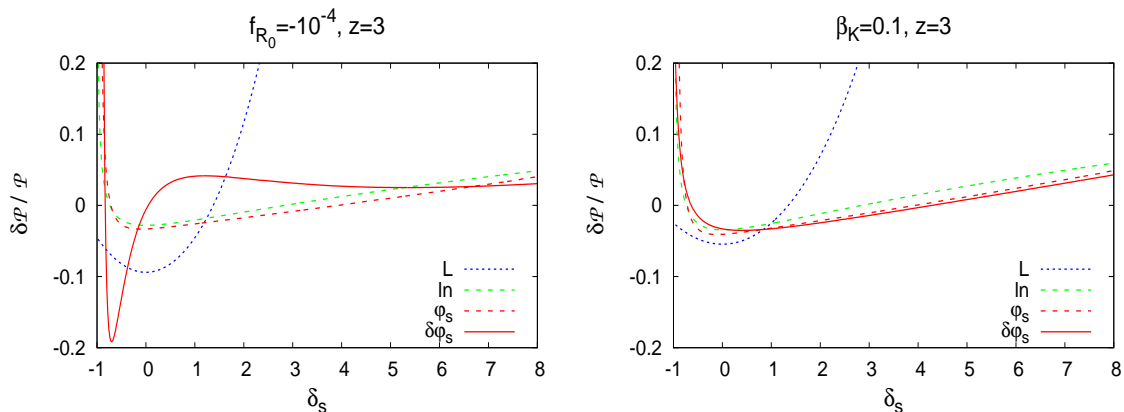


Figure 2. *Left panel:* relative deviation of the PDF $\mathcal{P}(\delta_s)$ for the $f(R)$ models. As in Fig. 1, we display the Gaussian PDF from linear theory (blue dotted line “L”), the lognormal approximation (green dashed line “ln”), and the gravitational PDF (3.5). For the latter, we consider the cases where we keep the LCDM generating function φ_s (red dashed line “ φ_s ”), or we use the new generating function determined by the modified-gravity spherical collapse (red solid line “ $\delta\varphi_s$ ”). *Right panel:* case of the K-mouflage model.

This leads to stronger tails for the PDF $\mathcal{P}(\delta_s)$, as large fluctuations are less rare, and hence to lower values of $\mathcal{P}(\delta_s)$ for moderate contrasts $\delta_s \simeq 0$ as all PDFs are normalized to unity. We recover this behavior in Fig. 2, with a positive deviation $\delta\mathcal{P}$ at large negative and positive density contrasts. Using either the lognormal approximation or the fixed LCDM generating function φ_s gives almost the same results for $\delta\mathcal{P}/\mathcal{P}$. This agrees with Fig. 1, which shows that the lognormal approximation and Eq.(3.5) lead to similar shapes, and the fact that in both cases the deviation only arises from the change of the matter density variance. For the $f(R)$ theories, the modification of the generating function φ_s , that is, of the higher-order normalized cumulants $\langle \delta_s^n \rangle_c / \sigma_s^{2(n-1)}$, has a significant impact. It strongly amplifies the deviation from the LCDM result for moderate density contrasts, $-0.8 \lesssim \delta_s \lesssim 3$. In contrast, for the K-mouflage model the modification of the generating function φ_s is small and it has a negligible impact on $\delta\mathcal{P}$. This expresses the fact that the K-mouflage gravitational dynamics is much closer to the LCDM case than the $f(R)$ theories. Indeed, as recalled in section 2.2, on these scales the K-mouflage scalar field ϕ is still in the linear regime (the nonlinear screening mechanism only appears at galactic scales and overdensities). Then, the only modification to gravitational processes is a slow time dependence of Newton’s constant. Clearly, this will not give rise to dramatic qualitative phenomena. In contrast, for the $f(R)$ theories there is a new scale dependence, set by $m(a)$, and the nonlinear regime of the modified gravity sector also becomes relevant faster. Besides, the coupling strength β is greater. Therefore, it is not surprising that gravitational processes deviate more strongly from the LCDM cosmology.

This can also be seen at the quantitative level in the coefficient ν_2 obtained from second-order perturbation theory, which would also enter the computation of bias parameters. Thus, if we decompose the initial linear density perturbation into a long wavelength mode δ_{Ll} and a short wavelength mode δ_{Ls} , $\delta_L = \delta_{Ll} + \delta_{Ls}$, higher-order perturbation theory $\delta \simeq \sum_n \delta_L^n$ gives rise to mode couplings. At second order in the density, and linear order in δ_{Ls} , this gives a

model	LCDM	$f_{R_0} = -10^{-4}$	$f_{R_0} = -10^{-5}$	$f_{R_0} = -10^{-6}$	$\beta_K = 0.1$
$\nu_2(k_s, 1h\text{Mpc}^{-1})$	1.62	1.65	1.65	1.64	1.62
$\nu_2(k_s, k_s)$	1.62	1.62	1.63	1.63	1.62

Table 1. Coefficient $\nu_2(k_1, k_2)$ for the LCDM, $f(R)$ and K-mouflage cosmologies, at $z = 3$. We show the cases $(k_1, k_2) = (k_s, 1h\text{Mpc}^{-1})$ (first row) and $k_1 = k_2 = k_s$ (second row).

contribution

$$\delta_s = (1 + \nu_2 \delta_{LI}) \delta_{Ls}, \quad (3.6)$$

which describes how small-scale perturbations are enhanced by large-scale modes. For the simple Einstein-de Sitter cosmology, this gives the well-known factor $\nu_2 = 34/21$ that also corresponds to the angular average of the second-order perturbation theory kernel $F_2(\mathbf{k}_1, \mathbf{k}_2)$ [38]. The expression (3.6) can also serve as a basis for the computation of bias parameters [39]. On the other hand, on large scales the skewness of the density contrast, which is the coefficient of the cubic term in the generating function $\varphi_s(y)$ and is defined by $S_3 = \langle \delta^3 \rangle_c / \sigma^4$, is given by $S_3 = 3\nu_2 + d \ln \sigma^2 / d \ln x$ [38]. We give in Eq.(B.1) in appendix B the expression of the angle-averaged coefficient $\nu_2(k_1, k_2)$ for general cosmologies.

We show the values of ν_2 in Table 1. For cosmologies with a scale dependence such as the $f(R)$ theories, it depends on wavenumbers. We show in the first row the case of the pair $(k_s, 1h\text{Mpc}^{-1})$, where k_s is the smoothing scale of Eq.(3.3). This describes the amplification of short-scale modes k_s by long-scale modes $k_l = 1h\text{Mpc}^{-1}$ as in Eq.(3.6). The second row corresponds to the single wavenumber k_s , which is relevant for the skewness of the density contrast at the single scale k_s . Because the modified-gravity theories we study here amplify and speed up the linear perturbations, they increase ν_2 and the skewness of the PDF $\mathcal{P}(\delta_s)$. For the scale-independent LCDM and K-mouflage cosmologies, the two rows are equal, while for the scale-dependent $f(R)$ theories the value is higher and further from the LCDM result in the first row, associated to different scales. This is because these $f(R)$ theories introduce a new dependence on the ratio k_1/k_2 . In agreement with Fig. 2, the deviation of ν_2 from the LCDM value is greater for the $f(R)$ theories than for the K-mouflage model, where it is below the percent level. This is due to the fact that the K-mouflage scalar field ϕ is still in the linear unscreened regime and that in this model $\delta\phi$ is an odd functional of δ , which implies $\gamma_{2;11}^s = 0$ for the new vertex that generically appears in Eq.(B.1) [40]. This explains the greater impact of the deviation of the cumulant generating function φ_s for the $f(R)$ theories.

3.3 $\mathcal{P}(F)$ for modified-gravity theories

We show in Fig. 3 the relative deviation of $\mathcal{P}(F)$ for the $f(R)$ theories and the K-mouflage model. As in the numerical simulations [14], in all cases we set the coefficient A in Eq.(3.2) so that the mean flux matches the observed value of [37], $\langle F \rangle = 0.72$. As for the density PDF shown in Fig. 2, the amplification of structure formation in the modified-gravity scenarios leads to stronger tails for $\mathcal{P}(F)$, and therefore to a lower amplitude of the PDF at the moderate values around $\langle F \rangle$.

For the $f(R)$ theories we roughly recover the order of magnitude and the shape of the deviation found in the numerical simulations [14]. However, the agreement is not very good and the simulation results fall between the two predictions obtained from Eq.(3.5), where we either neglect or include the impact of modified gravity on the generating function φ_s . This suggests that the exact result is between these two approximations. Indeed, the smoothing scale x_s is already in the mildly nonlinear regime, and the generating function φ_s may already

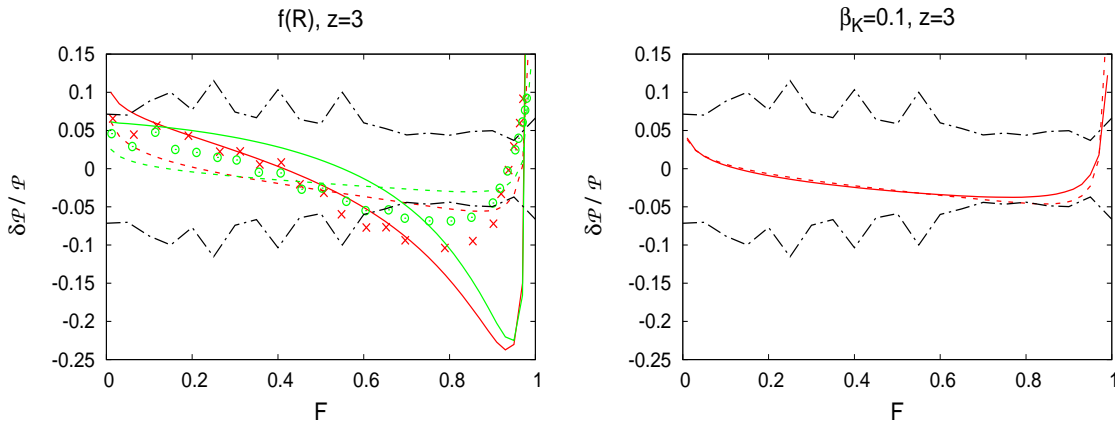


Figure 3. *Left panel:* relative deviation of the PDF $\mathcal{P}(F)$ for the $f(R)$ models $f_{R_0} = -10^{-4}$ (red lines) and $f_{R_0} = -10^{-5}$ (green lines). The points are the numerical simulations of [14] for $f_{R_0} = -10^{-4}$ (red crosses) and $f_{R_0} = -10^{-5}$ (green circles). As in Fig. 2, the dashed lines neglect the dependence on cosmology of the cumulant generating function while the solid lines use the modified generating function. The symmetric upper and lower black dot-dashed lines are the $\pm 1\sigma$ relative errors of the observational results of [37]. *Right panel:* relative deviation of the PDF $\mathcal{P}(F)$ for the K-mouflage model (red lines), with the $\pm 1\sigma$ relative observational errors of [37].

model	LCDM	$f_{R_0} = -10^{-4}$	$f_{R_0} = -10^{-5}$	$f_{R_0} = -10^{-6}$	$\beta_K = 0.1$
$\langle \delta_F^2 \rangle$	0.199	0.215	0.212	0.211	0.202
relative deviation	0	8%	7%	6%	1%

Table 2. *First row:* variance $\langle \delta_F^2 \rangle$ of the Lyman- α flux for the LCDM, $f(R)$ and K-mouflage cosmologies, at $z = 3$. *Second row:* relative deviation of $\langle \delta_F^2 \rangle$ from the LCDM prediction.

somewhat depart from its quasilinear value. In particular, the overestimate of the negative deviation at $F \simeq 0.9$ suggests that the negative deviation at $\delta_s \simeq -0.8$ in Fig. 2 was too large.

As the K-mouflage model is closer to the LCDM cosmology, in the sense that the linear growth rate does not depend on wave number and outside of galaxies the modification of gravity only corresponds to a small time dependence of Newton’s constant, we can expect our modeling of $\mathcal{P}(F)$ to fare better. In agreement with Fig. 2, the modification of φ_s has no impact on the PDF. Thus, our prediction should be more robust than for the $f(R)$ theories.

Another factor that can explain the discrepancies found in the left panel in Fig. 3 is our neglect of redshift-space effects. However, since the deviations are typically smaller than the 1σ errorbars of the observations, we do not try to extend our modeling of $\mathcal{P}(F)$ to redshift-space. Indeed, the small amplitude of $\delta\mathcal{P}/\mathcal{P}$ means that the Lyman- α flux PDF is not a competitive probe of these modified-gravity models.

We give in Table 2 the variance $\langle \delta_F^2 \rangle$ of the Lyman- α flux, with $\delta_F = F/\langle F \rangle - 1$. For the modified-gravity models we use the modified generating function $\delta\varphi_s$, which tends to overestimate the departure from the LCDM prediction. In agreement with the previous results, the relative deviation is smallest for the K-mouflage model, where it is only one percent.

4 Lyman- α flux decrement power spectrum

We now turn to the second Lyman- α statistics that we consider in this paper, the power spectrum $P_{\delta_F}(\mathbf{k})$ of the Lyman- α forest flux decrement $\delta_F = F/\langle F \rangle - 1$. Fitting formulas for $P_{\delta_F}(\mathbf{k})$ are usually written in terms of the power spectrum $P_L(k)$ of the linear matter density contrast at the same redshift, multiplied by several cutoffs and amplification factors [19, 41]. These factors account for several effects, such as the bias between the neutral hydrogen gas distribution and the total matter distribution, thermal broadening, redshift-space distortions, the nonlinear growth of density fluctuations, ..., and are obtained from fits to numerical simulations. In this paper, we also use such cutoffs, which we do not accurately predict but have realistic orders of magnitude and are fitted to simulations and observations. However, we do not introduce an ad-hoc amplification factor and we model the effects associated with the nonlinearity of the underlying density field by an analytical model based on a truncated Zeldovich approximation. This scheme cannot reach the accuracy of dedicated hydrodynamical numerical simulations, but we can hope that it captures some of the dependence on the primordial matter power spectrum and the growth of large-scale density perturbations.

4.1 IGM power spectrum $P_{\text{IGM}}(k)$

As in section 3 and Eq.(3.2) for the flux PDF, we follow the common description of the Lyman- α forest as due to fluctuations in a continuous intergalactic medium (IGM) [42–44] instead of a set of discrete objects. Thus, we first express the real-space IGM density power spectrum of the neutral hydrogen gas in terms of the primordial matter density power spectrum as

$$P_{\text{IGM}}(k) = P_{\text{Ztrunc}}(k) e^{-(k/k_s)^2}, \quad (4.1)$$

where $P_{\text{Ztrunc}}(k)$ is a truncated Zeldovich power spectrum [45–47] and k_s is the smoothing wave number introduced in Eq.(3.3). We define this truncated Zeldovich power spectrum as the standard Zeldovich power spectrum $P_Z(k)$ associated with a truncated linear power spectrum $P_{\text{Ltrunc}}(k)$, instead of the genuine primordial linear power spectrum $P_L(k)$,

$$P_{\text{Ztrunc}} = \max_{k_{\text{trunc}}} P_Z[P_{\text{Ltrunc}}] \quad \text{with} \quad P_{\text{Ltrunc}}(k) = P_L(k)/(1 + k^2/k_{\text{trunc}}^2)^2. \quad (4.2)$$

An alternative approach would be to use a lognormal model for the IGM density field, written as $\delta_{\text{IGM}} \propto e^{\delta_L}$, and to use simulations to obtain the statistical properties of this lognormal field [42]. The advantage of our approach (4.1) is that it directly provides the power spectrum, without the need of numerical simulations.

It has been noticed for a long time that using a truncated linear power spectrum instead of the full linear power spectrum in the Zeldovich mapping provides a better description of large-scale structures; it actually fares better than both the linear and lognormal approximations [48]. Indeed, the initial power at high wavenumbers gives rise to artificially large displacements in the Zeldovich mapping, where particles simply follow their linear trajectories. This leads to particles moving beyond collapsed structures, instead of turning back and oscillating in gravitational potential wells, which gives rise to a steep free-streaming cutoff of the predicted nonlinear power spectrum, instead of the actual amplification associated with the collapse into virialized halos. Then, truncating the initial power at high k reduces this effect and enables one to recover the structure of the cosmic web [48]. Of course, such a scheme cannot describe the inner parts of the virialized halos. However, this is well suited to

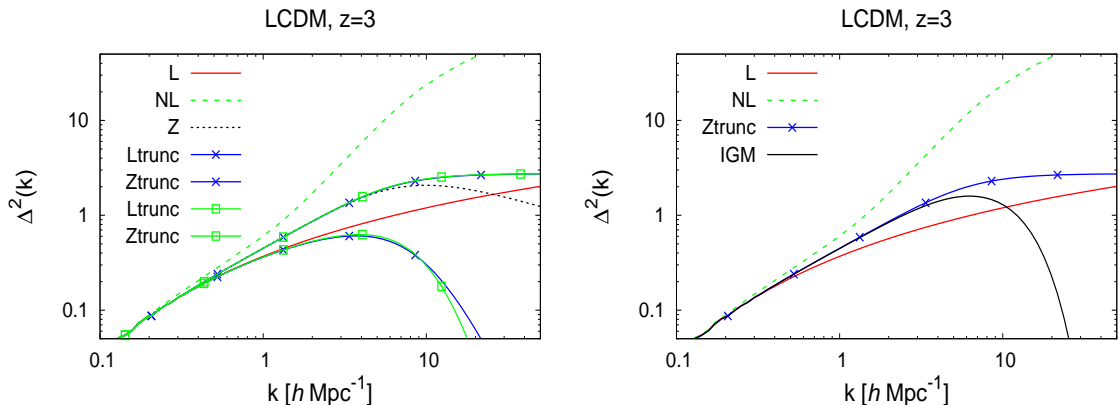


Figure 4. *Left panel:* logarithmic power $\Delta^2(k)$ for the linear power spectrum (L), a nonlinear model (NL), the standard Zeldovich approximation (Z), and two truncated linear power spectra (Ltrunc) and their associated Zeldovich approximations (Ztrunc). *Right panel:* the IGM model (4.1).

our purposes. Indeed, Lyman- α forest clouds consist of mildly nonlinear density fluctuations, typically associated with filaments or the outer parts of collapsed structures. Therefore, removing high-density collapsed regions is actually required to focus on the Lyman- α forest. The maximization in Eq.(4.2) means that the truncation wave number k_{trunc} that determines P_{Ltrunc} is defined as the one that maximizes $k^3 P_{\text{Ztrunc}}(k)$ at high k . Indeed, for large k_{trunc} , i.e. $k_{\text{trunc}} \gg k_{\text{NL}}$ where k_{NL} is the nonlinear transition scale with $\Delta_{\text{L}}^2(k) \sim 1$ ($\Delta^2 = 4\pi k^3 P$ is the logarithmic power that also measures the variance of density fluctuations at scale $1/k$), we recover the primordial linear power spectrum and the artificial smoothing of nonlinear structures. For small k_{trunc} , i.e. $k_{\text{trunc}} \ll k_{\text{NL}}$, we already remove power in the linear regime and prevent the formation of mildly nonlinear structures. For $k_{\text{trunc}} \sim k_{\text{NL}}$, we maximize the resulting Zeldovich power spectrum P_{Ztrunc} , which shows a universal tail $P_{\text{Ztrunc}}(k) \propto k^{-3}$, i.e. a flat $\Delta_{\text{Ztrunc}}^2(k)$ at high k . This captures the self-induced truncation of the mildly nonlinear density power spectrum we consider; the truncation is associated with the removal of high-density virialized regions, the formation of which is set by the onset of the nonlinear regime. This natural prescription also avoids introducing an additional free parameter k_{trunc} . This also ensures that the resulting power spectrum P_{Ztrunc} is not very sensitive to the form of the cutoff $1/(1 + k^2/k_{\text{trunc}}^2)^\nu$, where we could as well take $\nu = 1$ or 4 . Thus, we show in the left panel in Fig. 4 the power spectra obtained without truncation and with truncation, either with $\nu = 2$ (crosses) or $\nu = 4$ (squares). We can see that at redshift $z = 3$ the truncated Zeldovich approximation captures some of the nonlinear amplification of the matter density perturbations but saturates beyond $k_{\text{trunc}} \simeq 10 h \text{ Mpc}^{-1}$, as it does not describe the inner parts of collapsed halos. It mainly follows the standard Zeldovich approximation up to its peak and remains constant at higher k . We can check that the result is not sensitive to the exponent ν of the cutoff used for the truncation of the linear power spectrum.

Second, the cutoff $e^{-(k/k_s)^2}$ corresponds to the damping of density fluctuations in the gas by its nonzero pressure. We can see in the right panel in Fig. 4 the strong falloff at high- k beyond the Jeans wave number $k_s \sim 15 h \text{ Mpc}^{-1}$. However, this is a relatively small-scale effect and it does not impact the linear and weakly nonlinear growths of the IGM power spectrum. The power spectrum $P_{\text{IGM}}(k)$ shown in the right panel in Fig. 4 corresponds to the density

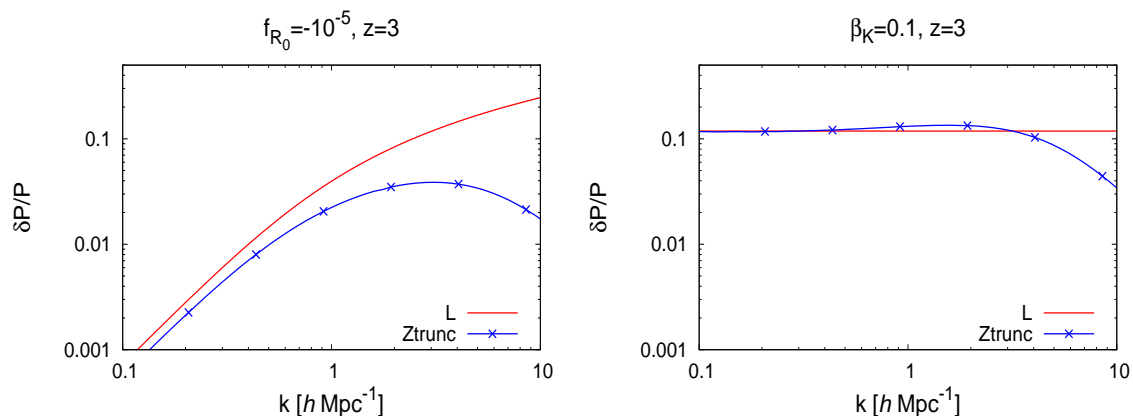


Figure 5. *Left panel:* relative deviation from the LCDM prediction of the matter power spectrum given by an $f(R)$ theory with $f_{R_0} = -10^{-5}$, at redshift $z = 3$. We show the linear power spectrum (L) and the truncated Zeldovich power spectrum (Ztrunc). *Right panel:* case of the K-mouflage model.

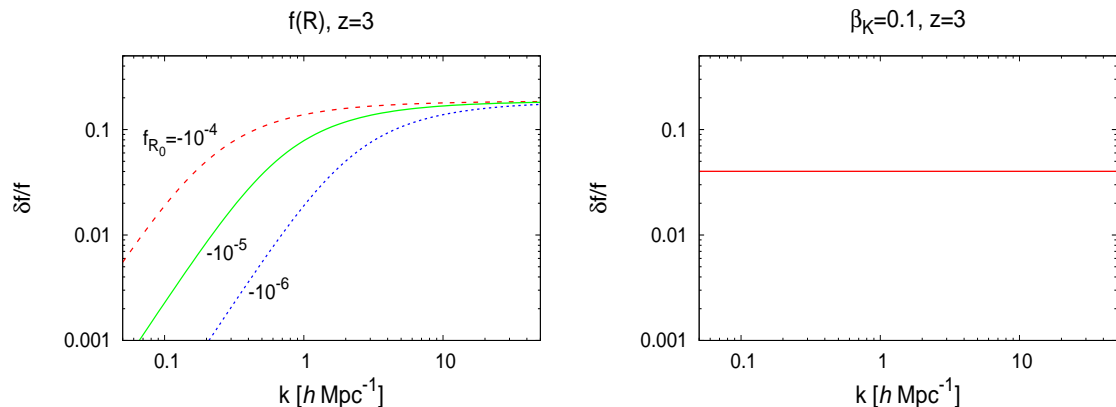


Figure 6. *Left panel:* relative deviation from the LCDM prediction of the growth rate f given by $f(R)$ theories, at redshift $z = 3$. *Right panel:* case of the K-mouflage model.

field δ_s with the PDF $\mathcal{P}(\delta_s)$ displayed in Fig. 1, which led to the flux PDF shown in Fig. 1.

4.2 Matter power spectrum for modified-gravity theories

We show in Fig. 5 the relative deviations of the linear and truncated Zeldovich power spectra from the LCDM prediction. The amplification of the growth of structure is due to the fifth force mediated by the scalar field, and in the K-mouflage model also to the running of Newton's constant with redshift, which now depends on the background value of the scalar field.

For the $f(R)$ theories, the relative deviation of $P_L(k)$ grows at higher k , because of the mass of the scalar field which yields a characteristic scale dependence of the linear growing mode. Moreover, at linear order there is no chameleon screening mechanism, which would reduce the deviation of the nonlinear power spectrum on small scales. The deviation of the truncated Zeldovich power spectrum peaks at the nonlinear scale and decreases at higher

k . This is due to the universal flat plateau already shown in Fig. 4. In practice, this also means that we do not need to include explicitly the nonlinear chameleon mechanism, as the deviation associated with nonlinear scales is already damped. Because we take the same IGM temperature for all cosmological scenarios, the relative deviation of the IGM power spectrum (4.1) coincides with that of the truncated Zeldovich power spectrum.

In contrast, for the K-mouflage scenario where the vanishing scalar-field mass prevents any scale dependence at linear order, the relative deviation of the linear matter power spectrum is independent of wave number. Then, the relative deviation of the truncated Zeldovich power spectrum is constant at low k and decreases again at high k because of its universal plateau.

We also show in Fig. 6 the relative deviations of the linear growth rate $f(k, a)$

$$f(k, a) = \frac{\partial \ln D_+(k, a)}{\partial \ln a}. \quad (4.3)$$

As for the linear power spectrum, the relative deviation of the growth rate $f(k, a)$ grows with k for the $f(R)$ theories, while it is scale independent for the K-mouflage model. As explained in section 2.1, smaller $|f_{R_0}|$ corresponds to a larger scalar field mass m and the deviation from the LCDM result is pushed to higher wave number, while the asymptotic value (in the linear regime) is fixed and set by $\beta = 1/\sqrt{6}$. For the K-mouflage model, the constant magnitude of $\delta P/P$ and $\delta f/f$ is directly set by the coupling constant β_K .

4.3 Lyman- α power spectrum $P_{\delta_F}(k)$

We assume that the Lyman- α flux-decrement power spectrum $P_{\delta_F}(\mathbf{k}, z)$ can be written in terms of the IGM density power spectrum P_{IGM} as

$$P_{\delta_F}(\mathbf{k}, z) = b_{\delta_F}^2 (1 + \beta\mu^2)^2 P_{\text{IGM}}(k) / (1 + f|k\mu|/k_{\text{NL}}) e^{-(k\mu/k_{\text{th}})^2}, \quad (4.4)$$

where $\mu = \mathbf{k} \cdot \mathbf{e}_z / k$ is the cosine of the wave number direction with respect to the line of sight, b_{δ_F} the bias, β the large-scale anisotropy parameter associated with redshift-space distortions, and k_{th} the thermal broadening cutoff wave number.

As recalled in section 3, even in the simplest picture the flux F is a nonlinear function of the smoothed matter density, as in Eq.(3.2). This makes the mapping from the matter density power spectrum to the flux power spectrum a complicated functional, and in general $P_{\delta_F}(k)$ depends on $P_L(k')$ for a range of wave numbers k' . On the other hand, on large scales, nonlinear local transformations preserve the correlation function, up to bias factors, which leads to a biased power spectrum up to an additive constant [49]. This applies to the Lyman- α power spectrum measured on length scales that are much greater than the smoothing scale x_s . This agrees with the fact that simulations show that the complicated transformation to the Lyman- α forest flux preserves the qualitative features of dark matter [22], which is why fitting formulae are usually written in terms of the linear matter power spectrum, with several fitted prefactors. This is also the motivation of Eq.(4.4), where $P_{\text{IGM}}(k)$ converges to $P_L(k)$ on large scales but becomes a nonlinear functional on small scales. Then, as in standard studies [22, 41], we calibrate the prefactors introduced in Eq.(4.4) by verifying that it agrees with numerical simulations for the 3D and 1D Lyman- α power spectrum of the LCDM cosmology, and for the 1D spectrum of the $f(R)$ theories. Then, we assume that this model also applies to the K-mouflage scenario. This is a reasonable assumption, as we found in section 3 that the small-scale Lyman- α physics (as measured by the one-point PDF $\mathcal{P}(F)$) of the K-mouflage

model is even closer to the LCDM case than the $f(R)$ theories. This is in particular seen in Tables 1 and 2. Moreover, all models that we consider remain very close to the LCDM cosmology.

The anisotropic μ -dependent terms arise from redshift-space distortions, due to the amplification or damping of fluctuations measured along the line of sight because of the radial velocity fluctuations. Indeed, the mapping from real space \mathbf{x} to redshift space \mathbf{s} writes as

$$\mathbf{s} = \mathbf{x} + \frac{v_{\parallel}}{aH} \mathbf{e}_z, \quad (4.5)$$

where v_{\parallel} is the radial peculiar velocity. Then, the velocity dispersion at a given position \mathbf{x} redistributes the matter at \mathbf{x} over a nonzero width along the radial redshift-space coordinate s_{\parallel} . This leads to a smoothing of real-space density fluctuations and a damping of the redshift-space power spectrum at high k . The factor $e^{-(k\mu/k_{\text{th}})^2}$ describes the smoothing by the thermal velocity dispersion, which we take to be Gaussian with the comoving wave number cutoff

$$k_{\text{th}} = \frac{aH}{b_{\text{th}}}, \quad b_{\text{th}} = \sqrt{\frac{k_{\text{B}}T}{2m_p}}, \quad (4.6)$$

where b_{th} is the thermal velocity dispersion [50]. The factor $1/(1 + f|k\mu|/k_{\text{NL}})$ describes the smoothing by the velocity dispersion due to the virialization of collapsed structures. On nonlinear scales, beyond k_{NL} , shell crossing appears and different velocity streams coexist at the same physical space location \mathbf{x} . This must again damp the redshift-space power spectrum. The factor f expresses that this damping appears earlier when the linear velocity perturbations are amplified with respect to the linear density field. The factor $(1 + \beta\mu^2)^2$ is the usual Kaiser effect [51], which describes that on large linear scales the single-stream velocity field amplifies the density perturbations, as matter is moving inward onto overdense regions. We simply take $\beta \simeq 1.3 f$, where $f(k, a)$ is the linear growth rate defined in Eq.(4.3). In principles, the factor β is defined as $\beta = fb_{\delta_F, \eta}/b_{\delta_F, \delta}$, where we distinguish the biases with respect to the linear density and velocity fields, $b_{\delta_F, \delta} = \partial\delta_F/\partial\delta$ and $b_{\delta_F, \eta} = \partial\delta_F/\partial\eta$, with $\eta = -(\partial v_{\parallel}/\partial x_{\parallel})/(aH)$ [39, 41]. At lowest order, these biases may be computed from mode couplings such as Eq.(3.6). However, we found that the analytical models for $b_{\delta_F, \delta}$ and $b_{\delta_F, \eta}$ [39, 52] do not fare very well. They do not improve the agreement with numerical simulations and are not very stable, in particular the large inaccuracies on $b_{\delta_F, \eta}$ can lead to artificially large or small values for β . This agrees with the results of [52], who pointed out that velocity effects and redshift-space distortions are very difficult to capture by simple analytical models. Therefore, we keep the simple expression $\beta \sim 1.3f$, which appears to be more robust and agrees with numerical simulations at redshift $z \simeq 3$ [41]. The very small departure of ν_2 from the LCDM result found in Table 1, especially for the K-mouflage model, suggests that this should be a reasonable approximation for the modified-gravity models we study in this paper. The prefactor $b_{\delta_F}^2$ is fitted to the observations. Apart from direct hydrodynamical simulations, an alternative would be to simulate the density and velocity fields associated with the truncated Zeldovich approximation, which allows a more accurate treatment of thermal and redshift-space distortions [43]. However, as we only wish to estimate the magnitude of the impact of modified-gravity theories, for simplicity we keep the analytical model (4.4). For precise measurements, one should in any case develop dedicated hydrodynamical simulations [44, 53, 54].

We show in the left panel in Fig. 7 the ratio of the Lyman- α power spectrum to the linear matter density power spectrum, at redshift $z = 3$ as a function of the wave number

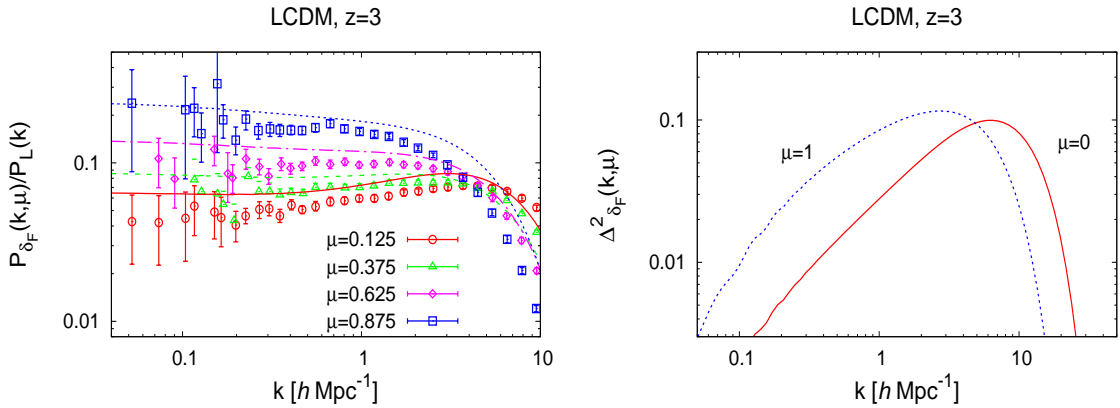


Figure 7. *Left panel:* ratio $P_{\delta_F}(k, \mu)/P_L(k)$ for $\mu = 0.125, 0.375, 0.625$ and 0.875 , from bottom to top. The symbols are the results of numerical simulations [41]. *Right panel:* logarithmic power spectrum $\Delta_{\delta_F}^2$ along the line of sight and perpendicular to the line of sight.

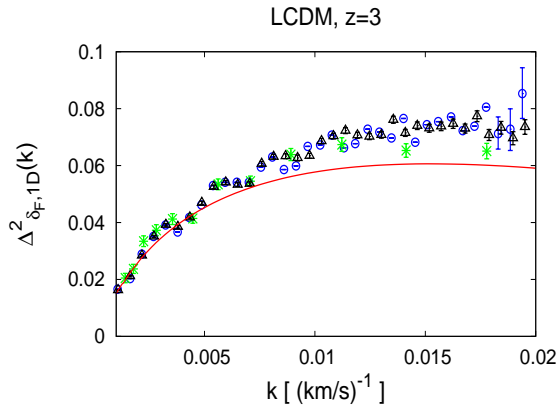


Figure 8. Logarithmic 1D power spectrum $\Delta_{\delta_F,1D}^2$. The data points are observations from [55] (stars), [56] (circles) and [57] (triangles). The solid line is our model.

k , for several values of μ . In agreement with Eq.(4.4), higher values of μ (i.e. directions increasingly parallel to the line of sight) amplify the power spectrum on large scales, because of the Kaiser effect, and damp the power on small scales because of the μ -dependent cutoffs, due to the smoothing by the velocity dispersion that arises from the thermal distribution and the gravitational multistreaming. The agreement with the numerical simulations [41] is not perfect, as expected for such a simple model as (4.4), but we recover the main trends and the magnitude of these redshift-space distortions. This suggests that our model captures the main processes at work. We show in the right panel in Fig. 7 the logarithmic power spectrum, $\Delta_{\delta_F}^2 = 4\pi k^3 P_{\delta_F}(k, \mu)$ for $\mu = 1$ and $\mu = 0$. In agreement with the left panel, the redshift-space distortions amplify the power at low k but give rise to a steeper falloff at high k .

The expression (4.4) gives the anisotropic 3D Lyman- α power spectrum, over all direc-

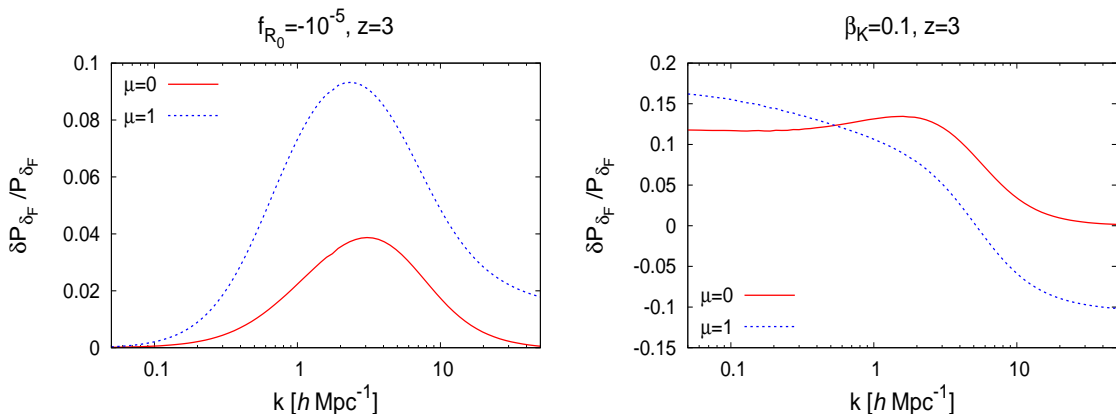


Figure 9. *Left panel:* relative deviation from the LCDM prediction of the 3D Lyman- α power spectra given by an $f(R)$ theory with $f_{R_0} = -10^{-5}$, at redshift $z = 3$, along directions orthogonal and parallel to the line of sight. *Right panel:* case of the K-mouflage model.

tions of \mathbf{k} . The observed 1D power spectrum along the line of sight is given by the standard integral

$$P_{\delta_F, 1D}(k_z) = \int_{-\infty}^{\infty} dk_x dk_y P_{\delta_F}(\mathbf{k}) = 2\pi \int_{k_z}^{\infty} dk k P_{\delta_F}(k, \mu = k_z/k). \quad (4.7)$$

This also defines the 1D logarithmic power as $\Delta_{\delta_F, 1D}^2(k) = (k/\pi)P_{\delta_F, 1D}(k)$, which we compare with observations [55–57] in Fig. 8. In agreement with Fig. 7, we recover the broad shape of the observed 1D Lyman- α power spectrum. The amplitude itself is not predicted, as the bias b_{δ_F} is fitted to these observations. The lack of power at high k , $k \gtrsim 0.015 (\text{km/s})^{-1}$ suggests some tension between the observations and the numerical simulations [41], as increasing the power at high k of the model would then worsen the agreement with the numerical simulations shown in Fig. 7. We do not tune our model to fit better the observations, to keep a reasonable agreement with both simulations and observations. This is likely to give a more robust framework. A more accurate modeling would require detailed comparisons between observations and simulations to better understand the different physical effects that enter the transformation from the linear matter density power spectrum to the Lyman- α power spectrum.

4.4 Lyman- α power spectrum for modified-gravity theories

We show in Fig. 9 the deviations with respect to the LCDM prediction for the 3D Lyman- α power spectra. For the $f(R)$ theories, we can see in the left panel that on large linear and weakly nonlinear scales the relative deviation of the Lyman- α power spectrum grows with k , following the rise of the modification to the matter power spectrum itself. The relative deviation is greater along the radial direction, which is also sensitive to the modification of the redshift-space factor f . The relative deviation of the transverse power spectrum decreases at higher k , following the behavior of the truncated Zeldovich power spectrum. Along the radial direction, the relative deviation does not decrease at high k and goes to a finite value. This is because it remains set by the change of the overall prefactor $(1 + \beta\mu^2)^2$ in Eq.(4.4), through the modification of the growth rate f . However, this result should not be trusted at nonlinear scales, $k \gtrsim 1h/\text{Mpc}$, because this simple form of the Kaiser amplification factor

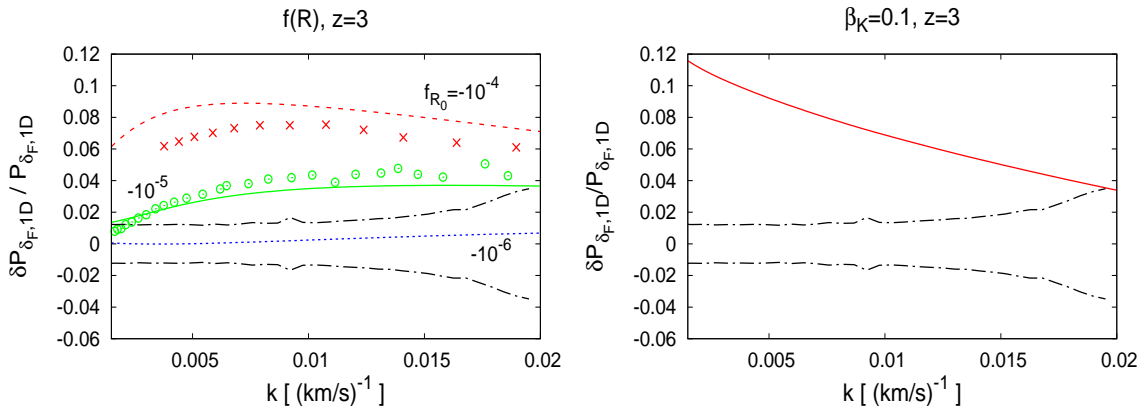


Figure 10. *Left panel:* relative deviation from the LCDM prediction of the 1D Lyman- α power spectrum at $z = 3$ given by $f(R)$ theories, with $f_{R_0} = -10^{-4}$ (red dashed line), -10^{-5} (green solid line) and -10^{-6} (blue dotted line). The points are the numerical simulations of [14] for $f_{R_0} = -10^{-4}$ (red crosses) and $f_{R_0} = -10^{-5}$ (green circles). The symmetric upper and lower black dot-dashed lines are the $\pm 1\sigma$ relative errors of the observational results of [57]. *Right panel:* case of the K-mouflage model.

only holds on linear scales. However, this range does not dominate the integral (4.7) that gives the 1D Lyman- α power spectrum.

For the K-mouflage model, the relative deviation of the Lyman- α power spectrum is scale independent on large linear and weakly nonlinear scales, as it is set by the relative deviation of the linear matter power spectrum. As for the $f(R)$ scenarios, the relative deviation of the transverse power spectrum decreases at high k , following the behavior of the truncated Zeldovich power spectrum. Along the radial direction, the relative deviation shows a faster decrease and even becomes negative at high k because of the numerator in Eq.(4.4), associated with the greater velocity dispersion. Again, this behavior should not be trusted as these scales are already in the highly nonlinear regime, which is not expected to be well described by our simple modeling.

We show in Fig. 10 the relative deviation of the 1D Lyman- α power spectrum. As compared with the 3D power spectra displayed in Fig. 9, the integration over the transverse wave numbers smoothes the relative deviation from the LCDM prediction. Thus, we obtain a deviation of order 4% for $f_{R_0} = -10^{-5}$, which does not vary much over $0.005 < k < 0.02 \text{ (km/s)}^{-1}$, and a deviation of order 7% for $f_{R_0} = -10^{-4}$. Our results agree reasonably well with the numerical simulations from [14], which suggests that the model captures the main dependence on the cosmology. The modest value of the deviation from the LCDM cosmology and the lack of salient features suggest that the Lyman- α power spectrum is not a competitive tool to constrain these $f(R)$ theories, which are already strongly constrained by astrophysical probes and Solar System tests of gravity that imply $|f_{R_0}| \lesssim 10^{-6}$. Thus, it appears that to obtain useful constraints on these scenarios one needs to reconstruct the 3D power spectrum, shown in Fig. 9, which shows a stronger scale dependence and a higher magnitude for the peak of the deviation from the LCDM power spectrum.

For the K-mouflage model, the 1D Lyman- α flux power spectrum shows a smooth relative deviation that slowly decreases with k . This is because of the scale independence for the

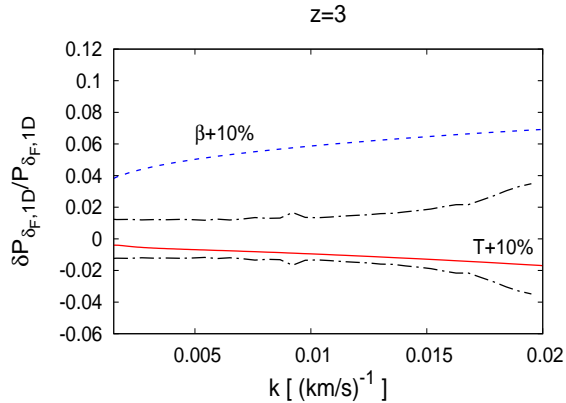


Figure 11. Relative deviation of the 1D Lyman- α power spectrum at $z = 3$ due to a 10% increase of the IGM temperature (red solid line) or a 10% increase of the redshift-space bias factor β (blue dashed line). The symmetric upper and lower black dot-dashed lines are the $\pm 1\sigma$ relative errors of the observational results of [57].

relative deviation of the linear matter power spectrum, due to the zero mass of the scalar field, while at high k nonlinear effects come into play that somewhat damp the dependence of the flux power spectrum on the underlying linear power spectrum. The comparison with the 1σ relative error of the observational results of [57] indicates that a precise analysis could constrain K-mouflage models at the level of $\beta_K \lesssim 0.1$. This can be compared for instance with CMB and background constraints, which give $\beta_K \lesssim 0.2$ [58]. Therefore, in contrast with the case of the $f(R)$ theories, the Lyman- α power spectrum could provide competitive constraints for these models. This is partly due to their different screening mechanisms. In the case of K-mouflage models, the nonlinear screening that ensures convergence to General Relativity in the Solar System has not impact on weakly nonlinear cosmological scales (because this corresponds to different regimes of the kinetic function $K(\chi)$ that are not necessarily related), and the tests of gravity in the Solar System or astrophysical environments only imply $\beta_K \lesssim 0.1$ (provided $K'(\chi)$ is sufficiently large in the small-scale quasistatic regime).

Obtaining competitive constraints would require a more accurate modeling, or at least a comparison with a set of K-mouflage numerical simulations to check the accuracy of our modeling, which we leave to future works. On the other hand, the rather large deviation found in Fig. 10, as compared with the small deviation of the one-point variance $\langle \delta_F^2 \rangle$ found in Table 2, suggests that our result is robust and would not be removed by the impact on the small-scale IGM physics.

The comparison with the case of the $f(R)$ theories also shows that the shape of the relative deviation of the Lyman- α flux power spectrum can provide useful constraints on the mass of the scalar field, or more generally on whether new length scales are introduced by a possible nonstandard cosmological scenario.

4.5 Degeneracies with physical parameters

To investigate the robustness of our results with respect to small-scale modifications of the IGM physics, we show in Fig. 11 the relative deviations of the 1D Lyman- α power spectrum for a 10% increase of the IGM temperature T or of the bias ratio β . The increased temperature

implies a stronger damping of the IGM power spectrum (4.1), because of the greater Jeans length scale, and of the Lyman- α power spectrum (4.4), because of the greater thermal broadening. As seen in Fig. 11, this yields a flat decrease of $P_{\delta_F,1D}(k)$ of about 1%. The increased factor β yields a flat increase of $P_{\delta_F,1D}(k)$ of about 6%, through Eq.(4.4). The comparison with Fig. 10 shows that the impact of these physical parameters remains modest and gives a scale dependence that is different from the modified-gravity models. This shows that it is possible to break degeneracies between such effects and modified gravity by using the scale dependence of the power spectrum.

5 Conclusion

In this paper, we have presented a simple modeling of the Lyman- α forest statistics to estimate the impact of two modified-gravity scenarios, the $f(R)$ and K-mouflage models.

We have first considered the probability distribution function $\mathcal{P}(F)$ of the Lyman- α flux. We find that this is not a very competitive probe of modified-gravity theories. It is also difficult to model analytically for scenarios that introduce a new scale dependence, such as the $f(R)$ theories, where the deviation of the PDF of the matter density contrast goes somewhat beyond the amplification of the variance and involves the higher-order cumulants.

Next, we have developed a simple modeling of the Lyman- α flux power spectrum, using a truncated Zeldovich approximation. This provides a good starting point to describe the Lyman- α power spectrum at $z \sim 3$, as it captures weakly nonlinear structures while removing the contributions of highly nonlinear objects that do not correspond to Lyman- α forest clouds. Taking into account thermal and redshift-space effects, through bias and cutoff factors, we obtain a reasonably good agreement with numerical simulations of the concordance Λ CDM model and with observations. For the $f(R)$ models, where numerical simulations are available, we also obtain a reasonable agreement with the numerical results. We find that because of the line of sight integration, the deviations from the Λ CDM prediction for the 1D Lyman- α power spectrum are modest and flat over the observed range of wave numbers. This will make it difficult to derive competitive constraints for these models, which are already very strongly constrained by astrophysical probes. In contrast, because of their different screening mechanism, the K-mouflage models are less strongly constrained by astrophysical probes, which only constrain the negative- χ range of $K(\chi)$ with the bound $\beta_K \lesssim 0.1$. There, we find that the Lyman- α power spectrum could provide competitive constraints as compared with CMB and background measurements. However, this would require numerical simulations to check the accuracy of the analytical modeling.

In addition, the 3D Lyman- α power spectrum shows a stronger scale dependence, which is sensitive to the details of the modified-gravity theory, in particular to its scale dependence (which typically arises from the scale associated with the mass of the new scalar field). Therefore, reconstructing the 3D power spectrum by correlating neighboring lines of sight [59–63] could provide a useful probe of alternative cosmologies.

Acknowledgments

This work is supported in part by the EU Horizon 2020 research and innovation programme under the Marie-Sklodowska grant No. 690575. This article is based upon work related to the COST Action CA15117 (CANTATA) supported by COST (European Cooperation in Science and Technology).

A Cumulant generating function

We introduced in Eq.(3.5) the generating function $\varphi(y)$ of the cumulants of the density field. The first expression is actually the inverse Laplace transform of $e^{-\varphi/\sigma^2}$, which means that $\varphi(y)$ is also defined as the Laplace transform of the PDF $\mathcal{P}(\delta)$,

$$e^{-\varphi(y)/\sigma^2} = \int_{-1}^{\infty} d\delta e^{-y\delta/\sigma^2} \mathcal{P}(\delta) = \langle e^{-y\delta/\sigma^2} \rangle = \int \mathcal{D}\delta_L e^{-y\delta[\delta_L]/\sigma^2} e^{-\frac{1}{2}\delta_L \cdot C_L^{-1} \cdot \delta_L}. \quad (\text{A.1})$$

In the last expression we wrote the average $\langle e^{-y\delta/\sigma^2} \rangle$ as a statistical path integral over the initial conditions, defined by the Gaussian linear density field $\delta_L(\mathbf{x})$ with its two-point correlation C_L . As described in [35, 36], in the limit $\sigma \rightarrow 0$ this integral is dominated by a spherically symmetric saddle point. This gives $\varphi(y)$ as the minimum

$$\varphi(y) = \min_{\delta_{Lq}} \left[y\mathcal{F}(\delta_{Lq}) + \frac{1}{2} \frac{\sigma_x^2}{\sigma_q^2} \delta_{Lq}^2 \right], \quad q = (1 + \delta)^{1/3} x, \quad (\text{A.2})$$

see also [64–66] for recent works. Here $\delta(x) = \mathcal{F}(\delta_{Lq})$ is the nonlinear density contrast at the scale x reached by the collapse of a linear density contrast δ_{Lq} at the Lagrangian scale q , and $q = (1 + \delta)^{1/3} x$ expresses the conservation of matter. The functional $\delta[\delta_L]$ is reduced to the spherically symmetric function $\mathcal{F}(\delta_{Lq})$ because for scale-independent gravity theories, such as General Relativity and the K-mouflage model (in its unscreened regime), different shells decouple in the spherical gravitational dynamics before shell crossing. The $f(R)$ theories introduce a scale dependence that implies that the dynamics of all shells are coupled. This makes the problem much more complex, but as in [36] we use a simple approximation where we only follow the collapse of the mass scale q and take a fixed ansatz for the radial profile at each time step. Then, the generating function φ associated with any modified-gravity scenario is determined by the new spherical-collapse mapping $\mathcal{F}(\delta_L)$, see [36] for details.

B Second-order perturbation theory

Expanding the matter density contrast δ in powers of the linear density contrast δ_{L0} extrapolated to $z = 0$, we can write the second-order term in Fourier space as

$$\begin{aligned} \delta^{(2)}(\mathbf{k}, \eta) = & \int_{-\infty}^{\eta} d\eta' \int d\mathbf{k}_1 d\mathbf{k}_2 \delta_D(\mathbf{k}_1 + \mathbf{k}_2 - \mathbf{k}) \delta_{L0}(\mathbf{k}_1) \delta_{L0}(\mathbf{k}_2) \left[R_{11}(k; \eta, \eta') \alpha(\mathbf{k}_1, \mathbf{k}_2) \right. \\ & \times \frac{\partial D_+}{\partial \eta}(k_1, \eta') D_+(k_2, \eta') + R_{12}(k; \eta, \eta') \left(\beta(\mathbf{k}_1, \mathbf{k}_2) \frac{\partial D_+}{\partial \eta}(k_1, \eta') \frac{\partial D_+}{\partial \eta}(k_2, \eta') \right. \\ & \left. \left. + \gamma_{2;11}^s(\mathbf{k}_1, \mathbf{k}_2; \eta') D_+(k_1, \eta') D_+(k_2, \eta') \right) \right], \end{aligned}$$

where we use the notations of [67]. Here $\eta = \ln a$, D_+ is the linear growing mode, which depends on wavenumber in $f(R)$ theories, R_{ij} are the linear theory response functions, and $\alpha(\mathbf{k}_1, \mathbf{k}_2)$ and $\beta(\mathbf{k}_1, \mathbf{k}_2)$ are the usual geometric kernels that arise from the continuity and Euler equations. The factor $\gamma_{2;11}^s$ is a new cubic vertex that arises from the fact that in modified-gravity theories the effective gravitational potential becomes a nonlinear functional of the matter density field (because of the contribution of the fifth force), and $\gamma_{2;11}^s$ gives the

quadratic contribution. Thus, we define the spherically symmetric coefficient

$$\begin{aligned} \nu_2(k_1, k_2) = & \frac{1}{D_+(k_1, \eta)D_+(k_2, \eta)} \int_{-\infty}^{\eta} d\eta' \int_{-1}^1 \frac{d\mu}{2} \left[R_{11}(k; \eta, \eta') \left(\alpha(\mathbf{k}_1, \mathbf{k}_2) \frac{\partial D_+}{\partial \eta}(k_1, \eta') D_+(k_2, \eta') \right. \right. \\ & + \alpha(\mathbf{k}_2, \mathbf{k}_1) \frac{\partial D_+}{\partial \eta}(k_2, \eta') D_+(k_1, \eta') \left. \right) + 2R_{12}(k; \eta, \eta') \left(\beta(\mathbf{k}_1, \mathbf{k}_2) \frac{\partial D_+}{\partial \eta}(k_1, \eta') \frac{\partial D_+}{\partial \eta}(k_2, \eta') \right. \\ & \left. \left. + \gamma_{2;11}^s(\mathbf{k}_1, \mathbf{k}_2; \eta') D_+(k_1, \eta') D_+(k_2, \eta') \right) \right], \end{aligned}$$

where $\mathbf{k} = \mathbf{k}_1 + \mathbf{k}_2$ and $\mu = (\mathbf{k}_1 \cdot \mathbf{k}_2)/(k_1 k_2)$. For $k_1 \gg k_2$ this gives the amplification by long modes k_2 of the small-scale modes $k \simeq k_1$, which provides the bias at lowest order of perturbation theory as in Eq.(3.6) [39]. For $k_1 = k_2$ this gives the leading-order contribution to the skewness $\langle \delta^3 \rangle_c / \langle \delta^2 \rangle_c^2$ at scale k_1 . For cosmologies that are scale independent, like LCDM and the K-mouflage model in the unscreened regime, ν_2 is independent of scale. For cosmologies that introduce new scales, such as the $f(R)$ theories, it depends on scale. In the case of the Einstein-de Sitter universe, we recover the usual coefficient $\nu_2 = 34/21$ [38].

C The Zeldovich approximation

In the Zeldovich approximation [45], particles initially at a position \mathbf{q} evolve along a trajectory $\mathbf{x}(t, \mathbf{q})$. The variances of the relative displacement between two initial points separated by $\Delta \mathbf{q}$ are given by

$$\sigma_{\parallel}^2(\Delta q) = 2 \int d\mathbf{k} [1 - \cos(k_{\parallel} \Delta q)] \frac{k_{\parallel}^2}{\mathbf{k}^4} P_L(k) \quad (\text{C.1})$$

along the initial separation, and

$$\sigma_{\perp}^2(\Delta q) = 2 \int d\mathbf{k} [1 - \cos(k_{\perp} \Delta q)] \frac{k_{\perp}^2}{\mathbf{k}^4} P_L(k) \quad (\text{C.2})$$

in the orthogonal direction. The linear power spectrum is given by $P_L(k)$. In the Zeldovich approximation, and for Gaussian initial conditions, this leads to the Zeldovich power spectrum [46, 47]

$$P_Z(k) = \int \frac{d\Delta \mathbf{q}}{(2\pi)^3} e^{ik\mu\Delta q - \frac{1}{2}k^2\mu^2\sigma_{\parallel}^2 - \frac{1}{2}k^2(1-\mu^2)\sigma_{\perp}^2}, \quad (\text{C.3})$$

where the directing cosine is defined as $\mu = (\mathbf{k} \cdot \Delta \mathbf{q})/(k\Delta q)$. In the main text we use a truncated Zeldovich power spectrum (4.2).

References

- [1] T. Clifton, P. G. Ferreira, A. Padilla and C. Skordis, *Modified Gravity and Cosmology*, *Phys. Rep.* **513** (2012) 1 [1106.2476].
- [2] S. F. Hassan and R. A. Rosen, *Bimetric Gravity from Ghost-free Massive Gravity*, *JHEP* **02** (2012) 126 [1109.3515].
- [3] C. de Rham, G. Gabadadze and A. J. Tolley, *Resummation of Massive Gravity*, *Phys. Rev. Lett.* **106** (2011) 231101 [1011.1232].
- [4] E. Babichev, C. Charmousis, G. Esposito-Farèse and A. Lehébel, *Stability of black holes and the speed of gravitational waves within self-tuning cosmological models*, *Phys. Rev. Lett.* **120** (2018) .

- [5] G. W. Horndeski, *Second-order scalar-tensor field equations in a four-dimensional space*, *Int.J.Theor.Phys.* **10** (1974) 363.
- [6] C. Deffayet, X. Gao, D. Steer and G. Zahariade, *From k-essence to generalised Galileons*, *Phys. Rev. D* **D84** (2011) 064039 [[1103.3260](#)].
- [7] J. Gleyzes, D. Langlois, F. Piazza and F. Vernizzi, *Healthy theories beyond Horndeski*, *Phys. Rev. Lett.* **114** (2015) 211101 [[1404.6495](#)].
- [8] P. Creminelli and F. Vernizzi, *Dark Energy after GW170817 and GRB170817A*, *Phys. Rev. Lett.* **119** (2017) 251302 [[1710.05877](#)].
- [9] J. Sakstein and B. Jain, *Implications of the neutron star merger gw170817 for cosmological scalar-tensor theories*, *Physical Review Letters* **119** (2017) .
- [10] Y. Akrami, P. Brax, A.-C. Davis and V. Vardanyan, *Neutron star merger gw170817 strongly constrains doubly coupled bigravity*, *Phys. Rev. D* **97** (2018) .
- [11] L. Lombriser, *Constraining chameleon models with cosmology*, *Annalen der Physik* **526** (2014) 259.
- [12] P. Brax and P. Valageas, *K-mouflage cosmology: The background evolution*, *Phys. Rev. D* **90** (2014) 023507 [[1403.5420](#)].
- [13] P. Brax, L. A. Rizzo and P. Valageas, *K-mouflage effects on clusters of galaxies*, *Phys. Rev. D* **92** (2015) 043519 [[1505.05671](#)].
- [14] C. Arnold, E. Puchwein and V. Springel, *The Lyman α forest in $f(R)$ modified gravity*, *Month. Not. Roy. Astron. Soc.* **448** (2015) 2275 [[1411.2600](#)].
- [15] V. K. Narayanan, D. N. Spergel, R. Davé and C.-P. Ma, *Constraints on the mass of warm dark matter particles and the shape of the linear power spectrum from the lyman α forest*, *Astroph. J.* **543** (2000) L103.
- [16] M. Viel, G. D. Becker, J. S. Bolton and M. G. Haehnelt, *Warm dark matter as a solution to the small scale crisis: New constraints from high redshift lyman- α forest data*, *Phys. Rev. D* **88** (2013) .
- [17] J. Baur, N. Palanque-Delabrouille, C. Yèche, C. Magneville and M. Viel, *Lyman-alpha forests cool warm dark matter*, *JCAP* **2016** (2016) 012.
- [18] V. Iršič, M. Viel, M. G. Haehnelt, J. S. Bolton and G. D. Becker, *First constraints on fuzzy dark matter from lyman- α forest data and hydrodynamical simulations*, *Phys. Rev. Lett.* **119** (2017) .
- [19] M. Garny, T. Konstandin, L. Sagunski and S. Tulin, *Lyman- α forest constraints on interacting dark sectors*, *JCAP* **2018** (2018) 011.
- [20] R. A. C. Croft, D. H. Weinberg, N. Katz and L. Hernquist, *Recovery of the power spectrum of mass fluctuations from observations of the lyman α forest*, *Astroph. J.* **495** (1998) 44.
- [21] R. A. C. Croft, D. H. Weinberg, M. Bolte, S. Burles, L. Hernquist, N. Katz et al., *Toward a precise measurement of matter clustering: Lyman α forest data at redshifts 2-4*, *Astroph. J.* **581** (2002) 20.
- [22] P. McDonald, *Toward a measurement of the cosmological geometry at $z \sim 2$: Predicting lyman α forest correlation in three dimensions and the potential of future data sets*, *Astroph. J.* **585** (2003) 34.
- [23] P. McDonald, U. Seljak, R. Cen, D. Shih, D. H. Weinberg, S. Burles et al., *The linear theory power spectrum from the lyman α forest in the sloan digital sky survey*, *Astroph. J.* **635** (2005) 761.
- [24] W. Hu and I. Sawicki, *Models of $f(R)$ Cosmic Acceleration that Evade Solar-System Tests*, *Phys. Rev.* **D76** (2007) 064004 [[0705.1158](#)].

- [25] J. Khoury and A. Weltman, *Chameleon fields: Awaiting surprises for tests of gravity in space*, *Phys. Rev. Lett.* **93** (2004) 171104 [[astro-ph/0309300](#)].
- [26] J. Khoury and A. Weltman, *Chameleon Cosmology*, *Phys. Rev.* **D69** (2004) 044026 [[astro-ph/0309411](#)].
- [27] E. Babichev, C. Deffayet and R. Ziour, *k-Mouflage gravity*, *Int.J.Mod.Phys.* **D18** (2009) 2147 [[0905.2943](#)].
- [28] P. Brax, C. Burrage and A.-C. Davis, *Screening fifth forces in k-essence and DBI models*, *JCAP* **01** (2013) 20 [[1209.1293](#)].
- [29] A. Barreira, P. Brax, S. Clesse, B. Li and P. Valageas, *K-mouflage gravity models that pass solar system and cosmological constraints*, *Phys. Rev. D* **91** (2015) .
- [30] J. E. Gunn and B. A. Peterson, *On the Density of Neutral Hydrogen in Intergalactic Space.*, *Astrophysical Journal* **142** (1965) 1633.
- [31] L. Hui and N. Y. Gnedin, *Equation of state of the photoionized intergalactic medium*, *Month. Not. Roy. Astron. Soc.* **292** (1997) 27.
- [32] M. McQuinn, A. Lidz, M. Zaldarriaga, L. Hernquist, P. F. Hopkins, S. Dutta et al., *He II Reionization and its Effect on the Intergalactic Medium*, *Astrophysical Journal* **694** (2009) 842 [[0807.2799](#)].
- [33] N. Y. Gnedin and L. Hui, *Probing the universe with the lyman α forest – i. hydrodynamics of the low-density intergalactic medium*, *Month. Not. Roy. Astron. Soc.* **296** (1998) 44.
- [34] M. Zaldarriaga, R. Scoccimarro and L. Hui, *Inferring the Linear Power Spectrum from the Lyman α Forest*, *Astroph. J.* **590** (2003) 1 [[arXiv:astro-ph/0111230](#)].
- [35] P. Valageas, *Dynamics of gravitational clustering. II. Steepest-descent method for the quasi-linear regime*, *Astron. and Astrophys.* **382** (2002) 412 [[arXiv:astro-ph/0107126](#)].
- [36] P. Brax and P. Valageas, *Structure formation in modified gravity scenarios*, *Phys. Rev. D* **86** (2012) 063512 [[1205.6583](#)].
- [37] F. Calura, E. Tescari, V. D’Odorico, M. Viel, S. Cristiani, T.-S. Kim et al., *The lyman \hat{I} s forest flux probability distribution at $z > 3$* , *Month. Not. Roy. Astron. Soc.* **422** (2012) 3019.
- [38] F. Bernardeau, S. Colombi, E. Gaztañaga and R. Scoccimarro, *Large-scale structure of the Universe and cosmological perturbation theory*, *Phys. Rep.* **367** (2002) 1 [[arXiv:astro-ph/0112551](#)].
- [39] U. Seljak, *Bias, redshift space distortions and primordial nongaussianity of nonlinear transformations: application to lyman- α forest*, *JCAP* **2012** (2012) 004.
- [40] P. Brax and P. Valageas, *K-mouflage cosmology: Formation of large-scale structures*, *Phys. Rev. D* **90** (2014) 023508 [[1403.5424](#)].
- [41] A. Arinyo-i Prats, J. Miralda-Escudé, M. Viel and R. Cen, *The non-linear power spectrum of the lyman alpha forest*, *JCAP* **2015** (2015) 017.
- [42] H. Bi and A. F. Davidsen, *Evolution of structure in the intergalactic medium and the nature of the lyman α forest*, *Astroph. J.* **479** (1997) 523.
- [43] L. Hui, N. Y. Gnedin and Y. Zhang, *The statistics of density peaks and the column density distribution of the lyman α forest*, *Astroph. J.* **486** (1997) 599.
- [44] S. Peirani, D. H. Weinberg, S. Colombi, J. Blaizot, Y. Dubois and C. Pichon, *Lymas: Predicting large-scale lyman α forest statistics from the dark matter density field*, *Astroph. J.* **784** (2014) 11.
- [45] Y. B. Zel’Dovich, *Gravitational instability: An approximate theory for large density perturbations.*, *Astron. and Astrophys.* **5** (1970) 84.

- [46] P. Schneider and M. Bartelmann, *The power spectrum of density fluctuations in the Zel'dovich approximation*, *Month. Not. Roy. Astron. Soc.* **273** (1995) 475.
- [47] A. N. Taylor and A. J. S. Hamilton, *Non-linear cosmological power spectra in real and redshift space*, *Month. Not. Roy. Astron. Soc.* **282** (1996) 767 [[arXiv:astro-ph/9604020](#)].
- [48] P. Coles, A. L. Melott and S. F. Shandarin, *Testing approximations for non-linear gravitational clustering*, *Month. Not. Roy. Astron. Soc.* **260** (1993) 765.
- [49] R. J. Scherrer and D. H. Weinberg, *Constraints on the effects of locally biased galaxy formation*, *The Astrophysical Journal* **504** (1998) 607.
- [50] A. Garzilli, T. Theuns and J. Schaye, *The broadening of Lyman- α forest absorption lines*, *Month. Not. Roy. Astron. Soc.* **450** (2015) 1465 [[1502.05715](#)].
- [51] N. Kaiser, *Clustering in real space and in redshift space*, *Month. Not. Roy. Astron. Soc.* **227** (1987) 1.
- [52] A. M. Cieplak and A. Slosar, *Towards physics responsible for large-scale lyman- α forest bias parameters*, *JCAP* **2016** (2016) 016.
- [53] G. Rossi, N. Palanque-Delabrouille, A. Borde, M. Viel, C. Yèche, J. S. Bolton et al., *Suite of hydrodynamical simulations for the Lyman- α forest with massive neutrinos*, *Astron. and Astrophys.* **567** (2014) A79 [[1401.6464](#)].
- [54] C. Lochhaas, D. H. Weinberg, S. Peirani, Y. Dubois, S. Colombi, J. Blaizot et al., *Modelling lyman α forest cross-correlations with lymas*, *Month. Not. Roy. Astron. Soc.* **461** (2016) 4353.
- [55] P. McDonald, U. Seljak, S. Burles, D. J. Schlegel, D. H. Weinberg, R. Cen et al., *The lyman α forest power spectrum from the sloan digital sky survey*, *Astroph. J. Supplement Series* **163** (2006) 80.
- [56] N. Palanque-Delabrouille, C. Yèche, A. Borde, J.-M. Le Goff, G. Rossi, M. Viel et al., *The one-dimensional lyman α forest power spectrum from boss*, *Astron. and Astrophys.* **559** (2013) A85.
- [57] S. Chabanier, N. Palanque-Delabrouille, C. Yèche, J.-M. Le Goff, E. Armengaud, J. Bautista et al., *The one-dimensional power spectrum from the SDSS DR14 Ly α forests*, *arXiv e-prints* (2018) [[1812.03554](#)].
- [58] G. Benevento, M. Raveri, A. Lazanu, N. Bartolo, M. Liguori, P. Brax et al., *K-mouflage Imprints on Cosmological Observables and Data Constraints*, *ArXiv e-prints* (2018) [[1809.09958](#)].
- [59] C. Pichon, J. Vergely, E. Rollinde, S. Colombi and P. Petitjean, *Inversion of the lyman α forest: three-dimensional investigation of the intergalactic medium*, *Month. Not. Roy. Astron. Soc.* **326** (2001) 597.
- [60] A. Slosar, A. Font-Ribera, M. M. Pieri, J. Rich, J.-M. L. Goff, É. Aubourg et al., *The lyman- α forest in three dimensions: measurements of large scale flux correlations from boss 1st-year data*, *JCAP* **2011** (2011) 001.
- [61] J. Cisewski, R. A. C. Croft, P. E. Freeman, C. R. Genovese, N. Khandai, M. Ozbek et al., *Non-parametric 3d map of the intergalactic medium using the lyman-alpha forest*, *Month. Not. Roy. Astron. Soc.* **440** (2014) 2599.
- [62] M. Ozbek, R. A. C. Croft and N. Khandai, *Large-scale 3d mapping of the intergalactic medium using the lyman α forest*, *Month. Not. Roy. Astron. Soc.* **456** (2016) 3610.
- [63] A. Font-Ribera, P. McDonald and A. Slosar, *How to estimate the 3d power spectrum of the lyman- α forest*, *JCAP* **2018** (2018) 003.

- [64] C. Uhlemann, S. Codis, C. Pichon, F. Bernardeau and P. Reimberg, *Back in the saddle: large-deviation statistics of the cosmic log-density field*, *Monthly Notices of the Royal Astronomical Society* **460** (2016) 1529.
- [65] F. Bernardeau and P. Reimberg, *Large deviation principle at play in large scale structure cosmology*, *Physical Review D* **94** (2016) .
- [66] M. M. Ivanov, A. A. Kaurov and S. Sibiryakov, *Non-perturbative probability distribution function for cosmological counts in cells*, *arXiv e-prints* (2018) [[1811.07913](#)].
- [67] P. Brax and P. Valageas, *Impact on the power spectrum of screening in modified gravity scenarios*, *Phys. Rev. D* **88** (2013) 023527 [[1305.5647](#)].